Turkish Journal of Electrical Engineering & Computer Sciences

http://journals.tubitak.gov.tr/elektrik/

Research Article

Turk J Elec Eng & Comp Sci
(2015) 23: 1173 – 1186

doi:10.3906/elk-1306-22

Robust speed controller design for induction motors based on IFOC and Kharitonov theorem

Bijan MOAVENI*, **Mojtaba KHORSHIDI**
School of Railway Engineering, Iran University of Science and Technology, Tehran, Iran

Received: 03.06.2013 • **Accepted/Published Online:** 01.08.2013 • **Printed:** 10.06.2015

Abstract: In this paper, robust PI controllers are designed to control the speed of induction motors based on a vector control strategy. The design methodology defines the robust stability and robust performance regions in the $k_p - k_i$ (PI controller coefficients) plane using the Kharitonov theorem. In the control system design procedure, a nonlinear induction motor is modeled as an uncertain linear model. The procedure of modeling the uncertainties is presented. The required scientific foundations for designing a robust PI controller are also introduced in the general case while the necessary equations are derived. In the final step, the design procedure for a special motor is presented thoroughly. The simulation results indicate the efficiency of the method.

Key words: Induction motor, speed control, indirect field oriented control, robust control, Kharitonov theorem

1. Introduction

Induction motors are among the most commonly used motors in industry due to their appropriate size, lower level of repair and maintenance, high efficiency, low cost, and high level of reliability [1]. The speed and torque control algorithms of these motors are very complicated because of the strong coupling that exists between the torque and the flux. Therefore, from the control science point of view, the analysis of these motors leads to a nonlinear multivariable and time-variant control problem. These properties make the controller design procedure difficult [2].

In the past years, various methods of controlling the motor speed have been investigated [3–15]. One of the widely used methods in this regard is the theory of vector control, which controls the torque and flux in separate channels [8]. The advances in semiconductor devices of power electronics and microprocessors have made a major contribution to this method [8]. This method, which is also known as field-oriented control (FOC), decomposes the stator current into flux and torque components, just like DC motor control methods. In this way, accurate control of the induction motor by the components in the field flux direction and the component perpendicular to it becomes possible. Depending on how the rotor flux angle is determined, vector control methods can be categorized as direct field-oriented control (DFOC) and indirect field-oriented control (IFOC). When it comes to application, the indirect method is generally used, because it uses fewer sensors and offers a higher level of reliability. In this control method, a dynamic model of the motor in the $d-q$ domain is utilized to convert the nonlinear coefficients of the differential equations into constant ones and also to enhance the control process efficiency [1]. The block diagram of the IFOC method is shown in Figure 1. This method, in its classic form, needs 3 PI controllers (2 for current control and 1 for speed control).

*Correspondence: b_moaveni@iust.ac.ir

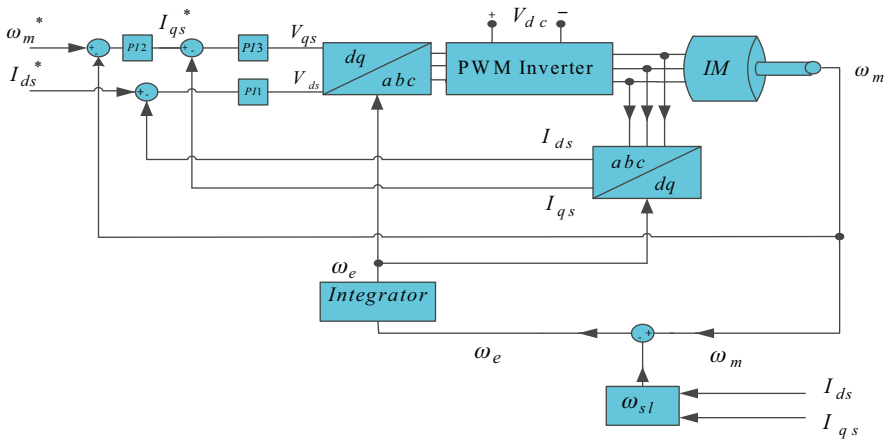

Figure 1. Block diagram of the IFOC method.

As shown in Figure 1, current is usually controlled in an inner loop, upon which the drive efficiency is highly dependent. Therefore, it is necessary to have a fast and accurate current controller to achieve appropriate dynamic and static performance [9]. In different papers various methods for designing an FOC current controller were reported; these methods include fuzzy sliding mode [10,12], deadbeat current controllers [11], artificial neural network controllers [15], multiobjective genetic fuzzy algorithms [13], and nonlinear controllers [14]. In [9], a sliding-mode current control scheme was presented for induction motor drives. This scheme used 2 sliding-mode controllers to regulate the d-axis and q-axis stator currents, respectively. This method exhibited several advantages, such as fast dynamic response, perfect decoupling, and robustness to parameter variations. In [10] and [12], a fuzzy sliding mode controller for IFOC was presented. It combined a sliding mode controller and a fuzzy controller to reduce the problems of conventional sliding mode control strategy. In [11], a current control scheme based on deadbeat control loops was presented. This method obtained good static and dynamic performances in both the simulation and experimental verifications. In [13], a multiobjective optimization method based on the genetic-fuzzy algorithm (GFA) was proposed. The GFA was employed to optimize the PI controller gains in the IFOC of an induction motor drive. The PI controller gains were designed to optimize the motor step response. In [14], the authors, by designing a nonlinear controller and a high gain speed estimator, presented a new speed-sensorless output feedback control for the full-order model of induction motors with unknown constant load torque on the basis of stator current measurements only. The main drawback of all these methods is their complications, which make them difficult to implement.

As introduced previously, induction motors are nonlinear and time-variant. Therefore, the aim of a few studies has been to design a robust control system that guarantees the closed-loop stability and desired performance in a robust manner. The topic of PI controller design has always been a subject of interest for control engineers; due to their relatively robust performance, simplicity of controller, applicability, and being conceivable for operators, PI controllers are widely used in various industries [16]. In recent years, important results in the field of robust control for uncertain linear systems based on the Kharitonov theorem have been presented [17].

Determining gains of PI controllers for induction motors is generally carried out using trial and error [10] or evolutionary algorithms, like the genetic algorithm, particle swarm optimization, or honey bee algorithms. The main shortcoming of these methods is that the boundaries of the search space are not known and this changes the optimal control problem to a suboptimal one.

In this paper, the design procedure of robust PI controllers that can guarantee the stability and performance of the motor under control is investigated. In the PI controller design methodology, we employ the Kharitonov theorem and its stability conditions. We also derive appropriate equations to determine the stabilizer PI parameters in the $k_p - k_i$ plane based on frequency response analysis. This method also conveniently calculates a space of PI controller parameters that results in appropriate performance of the closed-loop system.

After this brief introduction, the paper aims to provide information organized in the following sections. Section 2 presents the principle of the induction motor and IFOC. Section 3 covers the valuable equations for closed-loop stability of minimum phase transfer functions. In Section 4, stability regions that satisfy the desirable performance of the closed-loop system are introduced. In Section 5, the design procedure of the PI controller for uncertain systems is presented. Section 6 shows the design of PI controllers for the specified induction motor based on the Kharitonov theorem. Simulation results and conclusions are presented in Sections 7 and 8, respectively.

2. Induction motor and field-oriented control

FOC is a control technique that made AC drives equivalent to DC drives and it has become the industrial standard for high-performance motor applications due to its superior dynamic performance. Figure 1 shows the block diagram of the vector control method of an induction machine, where the torque and speed are controlled by 2 perpendicular components, field and armature currents, respectively.

The dynamic equations of an induction motor in the domain of the $d-q$ axis and in the synchronous reference frame are as given in Eqs. (1)–(5). These equations are for a squirrel cage induction motor with stator star connection considering linear magnetic circuit [8,18]. Table 1 lists all available variables of the induction motor.

Table 1. Variables of induction motor and their definitions.

$i_{qs}\,, i_{ds}$	$q-$ and $d-$axis stator currents	L_s	Inductance in stator phase
$V_{qs}\,, V_{ds}$	$q-$ and $d-$axis stator voltages	L_r	Inductance in rotor phase referenced to stator direction
$\lambda_{qr}\,, \lambda_{dr}$	$q-$ and $d-$axis rotor fluxes	ω_r	Rotational speed of the rotor
R_s	Resistance in stator phase	$T_r = {}^{L_r}/_{R_r}$	Time constant of the rotor
R_r	Resistance in rotor phase referenced to stator direction	$\sigma = 1 - \left({}^{L_m^2}/_{L_s L_r}\right)$	Leakage coefficient
L_m	Magnetizing inductance in phase	n_p	Number of pole pairs
J	Overall rotational inertia	B	Overall friction coefficient
T_l	External load torque of the motor	ω_e	Speed of rotating synchronous frame

$$\dot{i}_{ds} = -\left(\frac{R_s}{\sigma L_s} + \frac{1-\sigma}{\sigma T_r}\right) i_{qs} - \omega_e i_{ds} + \frac{L_m}{\sigma L_s L_r T_r}\lambda_{qr} - \frac{L_m \omega_r}{\sigma L_s L_r}\lambda_{dr} + \frac{1}{\sigma L_s} V_{qs} \tag{1}$$

$$\dot{i}_{ds} = -\left(\frac{R_s}{\sigma L_s} + \frac{1-\sigma}{\sigma T_r}\right) i_{ds} + \omega_e i_{qs} + \frac{L_m \omega_r}{\sigma L_s L_r}\lambda_{qr} + \frac{L_m}{\sigma L_s L_r T_r}\lambda_{dr} + \frac{1}{\sigma L_s} V_{ds} \tag{2}$$

$$\dot{\lambda}_{qr} = \frac{L_m}{T_r} i_{qs} - \frac{1}{T_r}\lambda_{qr} - (\omega_e - \omega_r)\,\lambda_{dr} \tag{3}$$

$$\dot{\lambda}_{qr} = \frac{L_m}{T_r} i_{ds} + (\omega_e - \omega_r)\,\lambda_{qr} - \frac{1}{T_r}\lambda_{dr} \tag{4}$$

$$T_e = \frac{3}{2} n_p \frac{L_m}{L_r} \left(\lambda_{dr} i_{qs} - \lambda_{qr} i_{ds}\right) = J\dot{\omega}_r + B\omega_r + T_l \tag{5}$$

To apply the IFOC method, the corresponding equations should be derived by putting (or fixing) the d-axis of the synchronous reference frame on the d-axis rotor flux vector (λ_{dr}) coaxially and setting the q-axis flux vector of the rotor (λ_{qr}) equal to zero. Consequently, the resulting components of the d-axis and q-axis of rotor flux are:

$$\begin{array}{l} \lambda_{qr} = 0 \\ \lambda_{dr} = \lambda_r \end{array} . \tag{6}$$

By applying the conditions in Eq. (6) to motor dynamic equations, the equations of the IFOC method are achieved as in Eqs. (7)–(9). From Eq. (3), the rotation slip speed can be found:

$$\omega_{sl} = \frac{L_m R_r}{L_r \lambda_r} i_{qs}, \tag{7}$$

and from Eq. (4) we have:

$$\lambda_r = \frac{L_m}{(1 + pT_r)} i_{ds}, \tag{8}$$

In Eq. (8), p is the differentiation operator. Since λ_r is kept constant during its operation $(p\lambda_r = 0)$, Eq. (8) can be rewritten as Eq. (9) [19]. In other words, the d-axis current of the stator can be used as the reference input instead of flux.

$$i_{ds}^* = \frac{\lambda_r^*}{L_m} \tag{9}$$

3. Closed-loop stability conditions of minimum phase plants using PI controllers

In this section, we derive appropriate equations to specify the regions of the $k_p - k_i$ plane that can provide closed-loop stability under PI controller action. Consider a SISO minimum-phase plant with transfer function, $G(s)$, and corresponding PI controller $C(s)$. The goal of the design procedure is to find all k_p and k_i that can result in closed-loop system stability.

$$C(s) = \frac{k_p s + k_i}{s} \tag{10}$$

According to the Nyquist stability criterion, one of the conditions of marginal stability is that the magnitude of open-loop transfer function must be equal to 1:

$$|G(j\omega)\, C(j\omega)| = 1. \tag{11}$$

Using Eqs. (10) and (11), we have:

$$|C(j\omega)| = \frac{1}{|G(j\omega)|} \rightarrow \left|\frac{j\omega k_p + k_i}{j\omega}\right| = \left|\frac{1}{G(j\omega)}\right| \rightarrow |j\omega k_p + k_i| = \frac{\omega}{|G(j\omega)|}. \tag{12}$$

Another condition for the closed-loop system to be marginally stable is that the open-loop system phase angle must be equal to $(2k+1)\pi$, $\forall k \in Z$.

$$\angle G(j\omega) + \angle C(j\omega) = (2k+1)\pi \tag{13}$$

Therefore, by using the PI controller phase characteristics, we have:

$$\angle G\left(j\omega\right)+\tan^{-1}\left(\frac{\omega k_p}{k_i}\right)-\frac{\pi}{2}=\left(2k+1\right)\pi\rightarrow\tan^{-1}\left(\frac{\omega k_p}{k_i}\right)=2k\pi+\frac{3\pi}{2}-\angle G\left(j\omega\right)\rightarrow$$

$$\frac{\omega k_p}{k_i}=\tan\left(2k\pi+\frac{3\pi}{2}-\angle G\left(j\omega\right)\right). \tag{14}$$

By using Eqs. (12) and (14), equations that can specify the marginal stability regions in terms of k_p and k_i can be expressed as:

$$\begin{cases}\frac{k_p}{k_i}=\frac{tan\left(2k\pi+\frac{3\pi}{2}-\angle G(j\omega)\right)}{\omega}\\ \omega^2k_p^2+k_i^2=\frac{\omega^2}{|G(j\omega)|^2}\end{cases}. \tag{15}$$

By simplifying Eq. (15), the governing conditions for marginal stability of the closed-loop control system are:

$$\begin{cases}k_i &= \frac{\omega}{|G\left(j\omega\right)|}\frac{1}{\sqrt{1+\tan^2\left(2k\pi+\frac{3\pi}{2}-\angle G\left(j\omega\right)\right)}}=\frac{\omega\cos\left(\angle G\left(j\omega\right)\right)}{|G\left(j\omega\right)|} & \text{(16a)}\\ k_p &= \frac{\tan\left(2k\pi+\frac{3\pi}{2}-\angle G\left(j\omega\right)\right)}{|G\left(j\omega\right)|\sqrt{1+\tan^2\left(2k\pi+\frac{3\pi}{2}-\angle G\left(j\omega\right)\right)}}=\frac{\sin\left(\angle G\left(j\omega\right)\right)}{|G\left(j\omega\right)|}. & \text{(16b)}\end{cases}$$

Eq. (16a) suggests that the line $k_i=0$ is a solution of this equation for zero frequency. Besides this one, other solutions may be found for Eq. (16) that can determine the boundaries for stable and unstable regions of the closed-loop system in the k_p-k_i plane. In order to determine the stable region, a test point may be utilized. A major characteristic of Eq. (16) is that, unlike other ones proposed in [17], the PI controller design is just dependent on magnitude and phase of the open-loop plant that can easily be available.

4. Robust stability and robust performance conditions

In control system design, in addition to satisfying the stability conditions, it is very important to achieve a desirable performance [15]. Desirable performance means having a time response in line with the designer's desired characteristics. In the frequency domain, desirable performance requires a reasonable gain margin, appropriate phase margin and bandwidth that are related to the upper bound of the sensitivity function, restriction of maximum overshoot in the time-domain response, and achievement of suitable settling time [20].

The objective of this section is to find regions in k_p-k_i that satisfy the desirable performance of the closed-loop system. To achieve an appropriate gain margin and phase margin, the following equation can be derived. If the system has a gain margin of A and a phase margin of φ, Eqs. (11) and (13) should be rewritten as:

$$\begin{cases}A\left|C\left(j\omega\right)G\left(j\omega\right)\right|=1\rightarrow\omega^2k_p^2+k_i^2=\frac{\omega^2}{A^2|G(j\omega)|^2}\\ \angle G\left(j\omega\right)C\left(j\omega\right)-\pi=\varphi\rightarrow\frac{k_p}{k_i}=\frac{\tan\left(2k\pi+\frac{3\pi}{2}-\angle G(j\omega)+\varphi\right)}{\omega}\end{cases}. \tag{17}$$

By simplifying Eq. (17), the boundary of a region in the k_p-k_i plane in which the gain margin and phase

margin of the system are in agreement with the designer's desired values can be found using Eq. (18).

$$\begin{cases} k_i = \frac{\omega \cos(\phi - \angle G(j\omega))}{A|G(j\omega)|} \\ k_p = \frac{\sin(\phi - \angle G(j\omega))}{A|G(j\omega)|} \end{cases} \tag{18}$$

These equations provide conditions related to suitable gain margin and phase margin simultaneously, while in [17], the aforementioned conditions have to be obtained separately each time.

As discussed earlier, the response speed or, in other words, the bandwidth of the closed-loop system is very important in the analysis and design of control systems. In [17], this was considered by moving all the closed-loop poles to the desired region in the s-plant. Here, however, we recommend bandwidth analysis. It is obvious that by increasing the system bandwidth, the settling time of the controlled system will decrease. We try to find a region in which all the values of k_p and k_i cause the system speed to remain at a desirable level. To obtain this goal, the designer's desired bandwidth (ω_{Bw}) is selected based on the settling time of desired time response, for which we have:

$$\left| \frac{G(j\omega_{Bw}) C(j\omega_{Bw})}{1 + G(j\omega_{Bw}) C(j\omega_{Bw})} \right| = \frac{\sqrt{2}}{2} \left| \frac{G(j0) C(j0)}{1 + G(j0) C(j0)} \right|. \tag{19}$$

As in this paper the PI controller has been used, Eq. (19) can be rewritten as:

$$\left| \frac{G(j\omega_{Bw}) (j\omega_{Bw} k_p + k_i)}{j\omega_{Bw} + G(j\omega_{Bw}) (j\omega_{Bw} k_p + k_i)} \right| = \frac{1}{\sqrt{2}}. \tag{20}$$

This equation can also be expressed as:

$$\sqrt{2} |G(j\omega_{Bw})| |j\omega_{Bw} k_p + k_i| = |j\omega_{Bw} + G(j\omega_{Bw}) (j\omega_{Bw} k_p + k_i)|.$$

Using the triangle inequality, we have

$$\begin{aligned} &\sqrt{2} |G(j\omega_{Bw})| |j\omega_{Bw} k_p + k_i| \leq |j\omega_{Bw}| + |G(j\omega_{Bw})| |(j\omega_{Bw} k_p + k_i)| \rightarrow \\ &|j\omega_{Bw} k_p + k_i| \leq \frac{|j\omega_{Bw}|}{(\sqrt{2}-1)|G(j\omega_{Bw})|} \end{aligned}, \tag{21}$$

where in the marginal state we have

$$\omega_{Bw}^2 k_p^2 + k_i^2 = \frac{\omega_{Bw}^2}{(\sqrt{2}-1) |G(j\omega_{Bw})|^2}. \tag{22}$$

Using Eq. (21), the regions of the $k_p - k_i$ plane in which the desired bandwidth is at an appropriate level can be obtained and Eq. (22) presents the boundary condition of the desired bandwidth region.

5. PI controller design for uncertain plants

Since most of the present systems in the real world are nonlinear [21], and modeling them as linear systems lacks accuracy, an uncertain linear modeling technique is used to model them. Uncertain linear modeling is

a useful approach in describing unmodeled dynamics, the alterations of the operating points, and changes in parameters due to the environmental conditions.

In these 2 recent decades, significant results regarding the stability analysis of uncertain systems have been presented [22–25]. In most control systems, the controller remains almost unchanged during the plant operation, while systems parameters undergo changes in a wide range. Thus, robustness of the controller against plant parameter changes is very important [21]. One of the theorems that are used in robust stability analysis is the Kharitonov theorem, which is discussed in the following text [17,21].

The Kharitonov theorem investigates the stability of uncertain linear systems by investigating the stability of 4 special polynomials, known as Kharitonov polynomials. If the characteristic equation of uncertain system is like Eq. (23), where its coefficients can vary in a specified range, the overall system is stable if and only if the 4 Kharitonov polynomials of Eq. (24) are Hurwitz.

$$P(s) = \sum_{i=0}^{n} d_i s^i \quad , \quad d_i^- \le d_i \le d_i^+ \tag{23}$$

$$\begin{aligned} P_1(s) &= d_0^- + d_1^- s + d_2^+ s^2 + d_3^+ s^3 + d_4^- s^4 + \cdots \\ P_2(s) &= d_0^- + d_1^+ s + d_2^+ s^2 + d_3^- s^3 + d_4^- s^4 + \cdots \\ P_3(s) &= d_0^+ + d_1^- s + d_2^- s^2 + d_3^+ s^3 + d_4^+ s^4 + \cdots \\ P_4(s) &= d_0^+ + d_1^+ s + d_2^- s^2 + d_3^- s^3 + d_4^+ s^4 + \cdots \end{aligned} \tag{24}$$

In this section, the method of calculating specific regions of the $k_p - k_i$ plane that guarantee the stability and desirable performance of uncertain systems is presented and investigated. Consider a system with the following uncertain transfer function:

$$G = \frac{N(s)}{D(s)} = \frac{a_0 + a_1 s + a_2 s^2 + \cdots + a_m s^m}{b_0 + b_1 s + b_2 s^2 + \cdots + b_n s^n}, \tag{25}$$

where $n \ge m$, $a_m \ne 0$, $b_n \ne 0$, $a_i \in \left[a_i^-, a_i^+\right]$, $b_i \in \left[b_i^-, b_i^+\right]$ [17]. The controller parameters k_p, k_i have to be designed so that it is possible to satisfy the desirable performance of the closed-loop system in addition to stability. This design is carried out based on the Kharitonov theorem. First, the Kharitonov polynomials related to the numerator and denominator of the transfer function are taken as follows.

$$\begin{aligned} N_1(s) &= a_0^- + a_1^- s + a_2^+ s^2 + a_3^+ s^3 + \cdots & D_1(s) &= b_0^- + b_1^- s + b_2^+ s^2 + b_3^+ s^3 + \cdots \\ N_2(s) &= a_0^- + a_1^+ s + a_2^+ s^2 + a_3^- s^3 + \cdots & D_2(s) &= b_0^- + b_1^+ s + b_2^+ s^2 + b_3^- s^3 + \cdots \\ N_3(s) &= a_0^+ + a_1^- s + a_2^- s^2 + a_3^+ s^3 + \cdots & D_3(s) &= b_0^+ + b_1^- s + b_2^- s^2 + b_3^+ s^3 + \cdots \\ N_4(s) &= a_0^+ + a_1^+ s + a_2^- s^2 + a_3^- s^3 + \cdots & D_4(s) &= b_0^+ + b_1^+ s + b_2^- s^2 + b_3^- s^3 + \cdots \end{aligned}$$

All the possible combinations of numerators and denominators will give 16 open-loop transfer functions $(M_t,\ t = 1, 2, \ldots, 16)$ as shown below, which are called Kharitonov transfer functions.

$$G_k(s) = G_{ij}(s) = \frac{N_i(s)}{D_j(s)} \quad , \quad i, j = 1, 2, 3, 4 \tag{26}$$

$$M_t(s) = C(s)\, G_{ij}(s) \quad , \quad t = 1, 2, \cdots, 16 \tag{27}$$

It can be proved that if a controller is capable of satisfying the stability of the 16 Kharitonov transfer functions and maintaining their performance at a suitable level, it can guarantee the stability and desirable performance of the uncertain system [17]. Consequently, these 16 transfer functions may be used to design an appropriate controller for the whole uncertain system with robust stability and performance. Using Eq. (16), the $k_p - k_i$ regions related to uncertain closed-loop system stability can be found from the overlapping stability regions resulting from Eq. (28).

$$\begin{cases} k_i = \frac{\omega \sin(\angle G_{ij}(j\omega))}{|G_{ij}(j\omega)|} \\ k_p = \frac{\cos(\angle G_{ij}(j\omega))}{|G_{ij}(j\omega)|} \end{cases} \quad i,j = 1,2,3,4 \tag{28}$$

Using Eq. (18), Eq. (29) can be utilized to find the regions that guarantee the robust performance of the closed-loop system corresponding to the 16 transfer functions in the $k_p - k_i$ plane.

$$\begin{cases} k_i = \frac{\omega \sin(\angle G_{ij}(j\omega)+\varphi)}{A|G_{ij}(j\omega)|} \\ k_p = \frac{\cos(\angle G_{ij}(j\omega)+\varphi)}{A|G_{ij}|} \end{cases} \quad i,j = 1,2,3,4 \tag{29}$$

Finally, from Eq. (21), the region related to the desirable robust bandwidth can be found.

$$|j\omega_{Bw}k_p + k_i| \leq \frac{|j\omega_{Bw}|}{\left(\sqrt{2}-1\right)\left|G_{ij}\left(j\omega_{Bw}\right)\right|^2} i,j = 1,2,3,4 \tag{30}$$

The overlapping region obtained by Eq. (30) is related to guaranteeing the closed-loop system response speed.

6. Designing the robust PI controllers for the IFOC method

In the IFOC method, 3 PI controllers exist. Two of them are used to generate q-axis voltage and one of them is used to generate d-axis voltage. The design of these PI controllers is done in a special order. First, the PI_1 and PI_3 controllers of Figure 1 are designed, and then the same procedure is done for the PI_2 controller. To design the PI controllers, the transfer function relating the input and output for each case has to be determined.

The induction motor, in addition to being nonlinear, includes variations in parameters during the motor operation. The variations in motor parameters take place due to heating and influence the resistance of the rotor and stator in such a way that the rotor resistance can vary up to 100% and the stator up to 50% [26]. Due to the highly nonlinear dynamics of the induction motor [2] (Eqs. (1)–(5)), the linearization process and uncertainty modeling are carried out using multiple-model modeling approaches [27].

For this purpose, the time response of the induction motor, from the starting time until reaching the steady state, has been divided into several parts, and for each part an equivalent linear model has been calculated and presented. This modeling in the simulation contributes to 13 linear transfer functions. The first transfer function models a portion of model startup, and by transferring the initial conditions to the second model, the response is modeled by a new linear model. This process goes on to reach its steady state. By comparing the 13 transfer functions, an uncertain linear model is obtained. As understood from induction motor Eqs. (1) through (5), it is clear that this motor is a system of order 5 and, therefore, it can be modeled by a linear transfer function with order 5 as in Eq. (31).

$$Induction\ motor\ transfer\ function \equiv \frac{output}{input} = \frac{a_0 + a_1 s + a_2 s^2 + a_3 s^3 + a_4 s^4}{b_0 + b_1 s + b_2 s^2 + b_3 s^3 + b_4 s^4 + b_5 s^5} \tag{31}$$

The uncertainty ranges of parameters can be stated as follows:

$$a_i \in \left[a_i^-, a_i^+\right], i = 0, 1, ..., 4,$$

$$b_j \in \left[b_j^-, b_j^+\right], j = 0, 1, ..., 5.$$

7. Simulation results

In this section, the proposed robust PI controller design procedure is applied to a typical induction motor and the results are presented, accordingly. The motor under study is a 2300 V motor and its parameters are listed in Table 2 [1].

7.1. Designing the first PI controller (PI_1)

Figure 2 presents and compares time responses of the induction motor based on the nonlinear model and linear multiple models. The results are similar to each other. However, to show the modeling accuracy, time responses at 3 points, m1, m2, and m3, have been magnified.

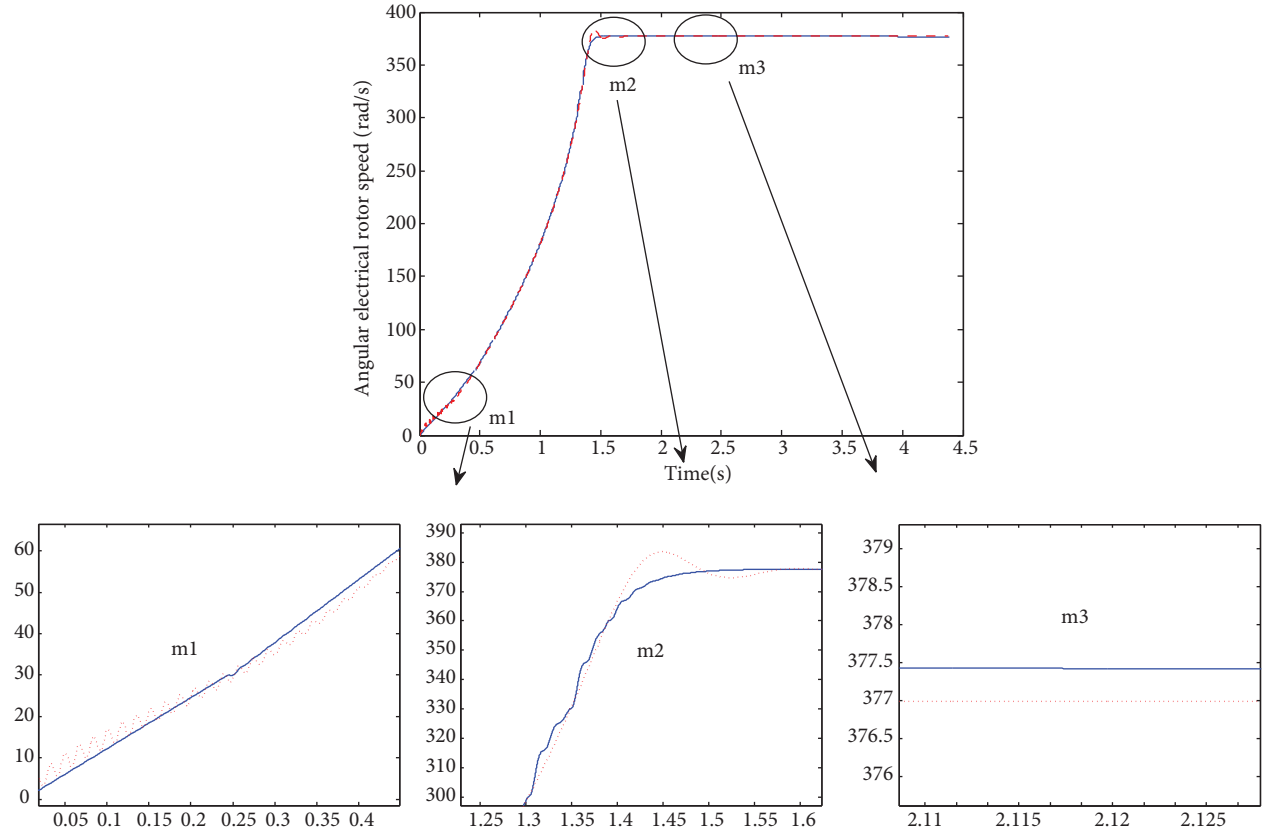

Figure 2. Time responses of nonlinear and linearized model for an induction motor. Solid line (blue) is the time response of linearized model and dashed line (Red) is the time response of nonlinear model.

Therefore, the transfer function of q-axis current can be presented as follows:

$$g = \frac{i_{qs}}{i_{qs}} = \frac{375660s^4 + 27133000s^3 + a_2s^2 + a_1s + a_0}{s^5 + 141.9s^4 + b_3s^3 + b_2s^2 + b_1s + b_0} \tag{32}$$

Table 2. Parameters of a 3-phase induction motor in $d-q$ domain.

Parameter	Value	Parameter	Value
$R_s(\Omega)$	0.262	$J(kg.m^2)$	11.06
$R_r(\Omega)$	0.187	$L_m(H)$	0.143
$L_s(H)$	0.0032	$f(Hz)$	60
$L_r(H)$	0.0032	n_P	4

In this equation, uncertain parameters are varied in the following intervals.

$$\begin{array}{ll} a_2 \in [20911000000,\ 20966000000] & b_3 \in [203110,\ 204990] \\ a_1 \in [330660000000,\ 1499900000000] & b_2 \in [12366000,\ 12500000] \\ a_0 \in [373220000000,\ 1845500000000] & b_1 \in [8035500000,\ 8316600000] \\ & b_0 \in [233990000000,\ 242110000000] \end{array} \tag{33}$$

Therefore, in a similar way, 16 open-loop Kharitonov transfer functions ($g_{ij},\ i,j=1,2,3,4$) can be obtained using Eqs. (26), (32), and (33). To show the presence of uncertainty in the model of the induction motor and its effect, bode diagrams of some transfer functions (g_{ij}) are shown in Figure 3.

The stability region of the first controller (PI_1) has been obtained using Eq. (28). The shaded region in Figure 4 shows a region of k_p-k_i in which the corresponding PI_1 controller can stabilize all $g_{ij},\ i,j=1,2,3,4$.

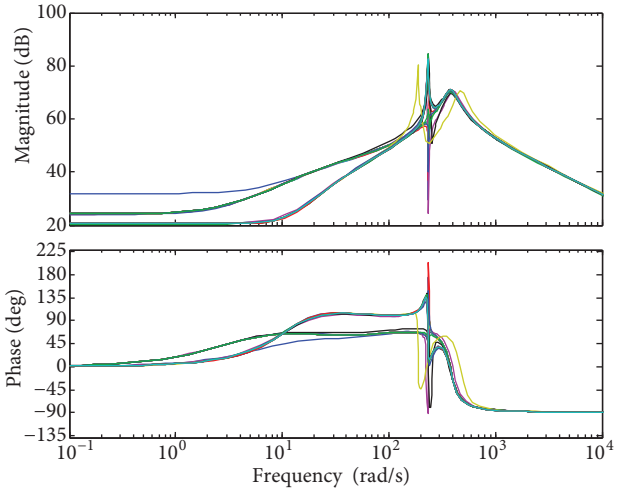

Figure 3. Bode diagram of the Kharitonov transfer functions for assumed induction motor.

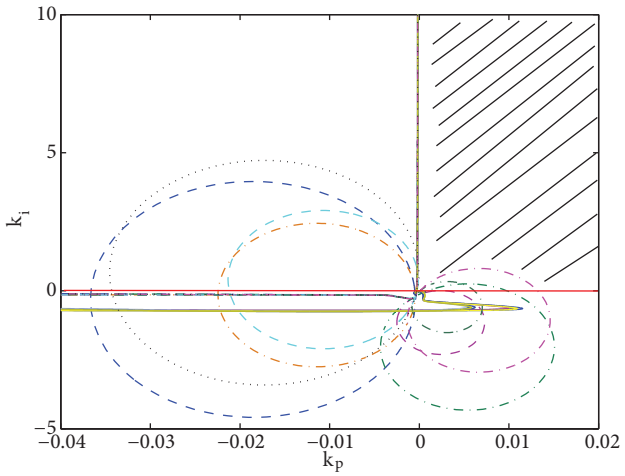

Figure 4. Closed-loop robust stability region (hatched area) in k_p-k_i (coefficients of PI_1 controller) plane.

In order to achieve robust performance, desirable features should be presented and the corresponding regions need to be extracted, accordingly. The design assumptions are as follows:

1. The upper limit sensitivity function must be lower than 0.4. In other words, it is necessary that $\left\|(1+G_{ij}(j\omega)C(j\omega))^{-1}\right\| < 0.4$. This condition guarantees the low sensitivity of the closed-loop transfer function against the open-loop transfer function variations. Thus, the appropriate gain margin will be above 0.7 and so we consider $A=\frac{\sqrt{2}}{2}$ in the simulation.

2. Desirable maximum percent overshoot has been considered as less than 10% in this paper. Therefore, the

damping ratio needs to be greater than 0.6, and consequently the minimum desirable phase margin will be $\varphi = \frac{\pi}{3}(rad)$.

3. The induction motor with the parameters listed in Table 2 will achieve its nominal speed within 1.5 s in free acceleration. We therefore consider the desirable settling time as less than or equal to 1.5 s under control. Thus, the desirable bandwidth will be greater than 4 rad/s.

Figure 5 shows the shaded region in the $k_p - k_i$ plane that satisfies the gain margin and phase margin constraints.

The desirable speed region can be defined by using Eq. (30). Notice that this region should be in the stable region of the PI_1 controller. Figure 6 shows a shaded region that satisfies the bandwidth constraint.

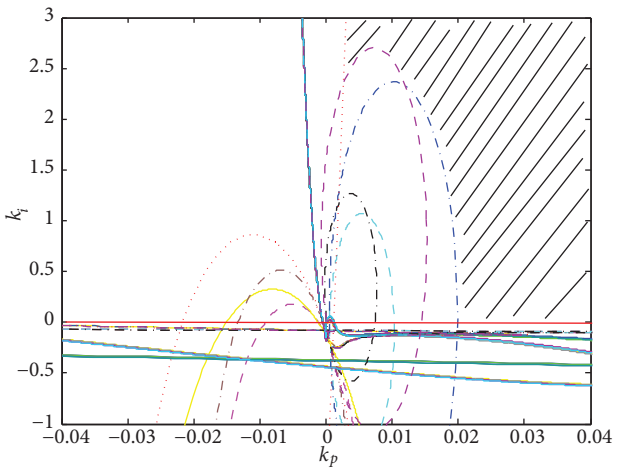

Figure 5. Closed-loop robust stability and robust performance region (hatched area) in $k_p - k_i$ (coefficients of PI_1 controller) for specified gain and phase margin.

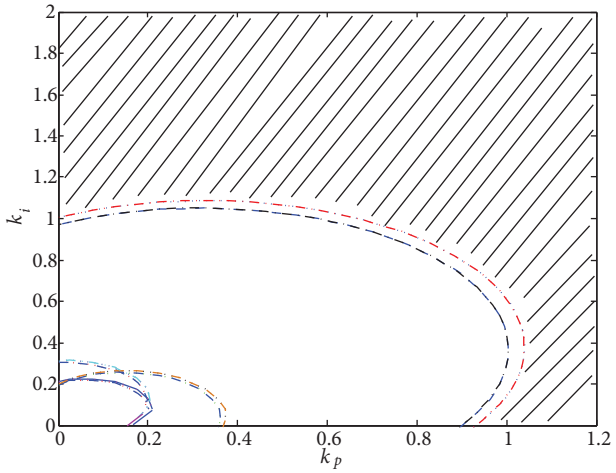

Figure 6. Closed-loop robust bandwidth region (hatched area) in $k_p - k_i$ (coefficients of PI_1 controller) plane.

Now parameters k_p and k_i of the robust PI controller should be chosen in the common shaded regions of Figures 4, 5, and 6. Therefore, we recommend PI_1 as in Eq. (34).

$$PI_1 = \frac{30s + 50}{s} \tag{34}$$

The step response of the nonlinear system to the designed controller is shown in Figure 7. It can be said that the design goals have been achieved by the PI_1 controller completely.

7.2. Designing the third PI controller (PI_3)

Since the state-space equation matrix of the symmetrical 3-phase induction motor is symmetric, transfer functions $\frac{I_{qs}}{V_{qs}}, \frac{I_{ds}}{V_{ds}}$ will be similar. As a result, the transfer function of this controller is the same as in Eq. (34) and the result will be similar to the responses shown in Figures 3–7.

7.3. Designing the second PI controller (PI_2)

Design of the second controller has been performed with a similar process. Interior loops of the PI_1 and PI_3 controllers are closed and the transfer function of $\frac{\omega_m}{I_{qs}}$ will be obtained, accordingly. The design process for this

controller is similar to the design of the PI_1 and PI_3 controllers. The corresponding desired regions have been shown in Figures 8–10.

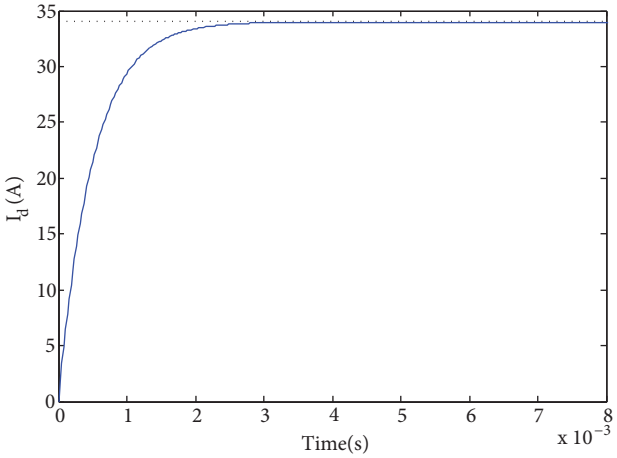

Figure 7. Time response of d-axis stator current in the presence of PI_1 controller.

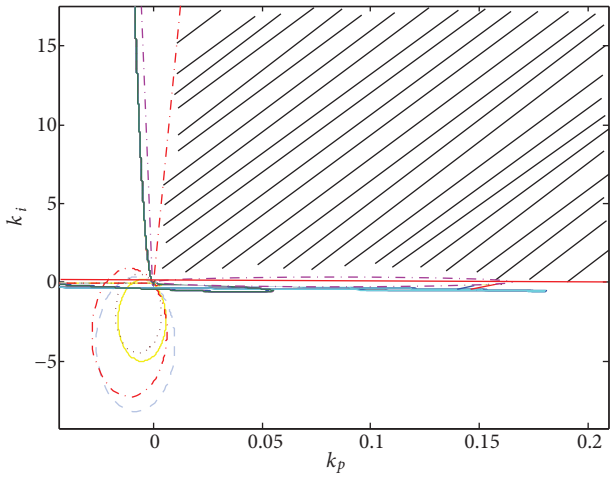

Figure 8. Closed-loop robust stability region (hatched area) in $k_p - k_i$ (coefficients of PI_2 controller) plane.

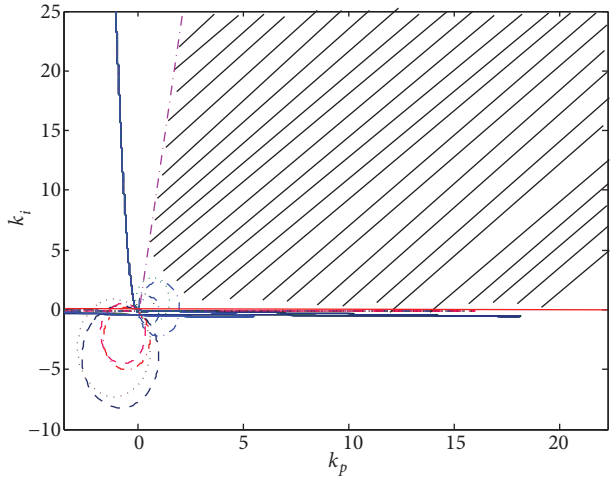

Figure 9. Closed-loop robust performance region (hatched area) in $k_p - k_i$ (coefficients of PI_2 controller) plane.

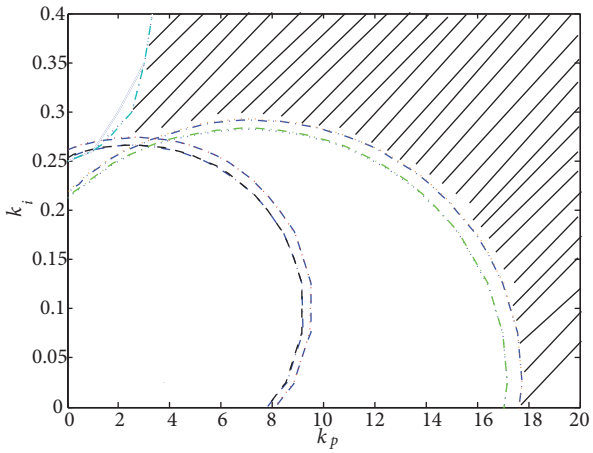

Figure 10. Closed-loop robust bandwidth region (hatched area) in $k_p - k_i$ (coefficient of PI_2 controller) plane.

The desirable rotor speed for this induction motor is assumed as 100 rad/s. According to Figures 8–10, we choose the coefficients of PI_2 as (35):

$$PI_2 = \frac{50s + 250}{s}. \tag{35}$$

Time responses of the controlled induction motor are shown in Figure 11. As can be seen in Figure 11, all design aims have been achieved using controllers PI_1, PI_2, and PI_3.

To evaluate the robustness of the IFOC method, the rotor and stator resistances have been changed up to 100% and 50%, respectively, and corresponding step responses are shown in Figure 12. It can be seen that the motor under control has a desirable performance.

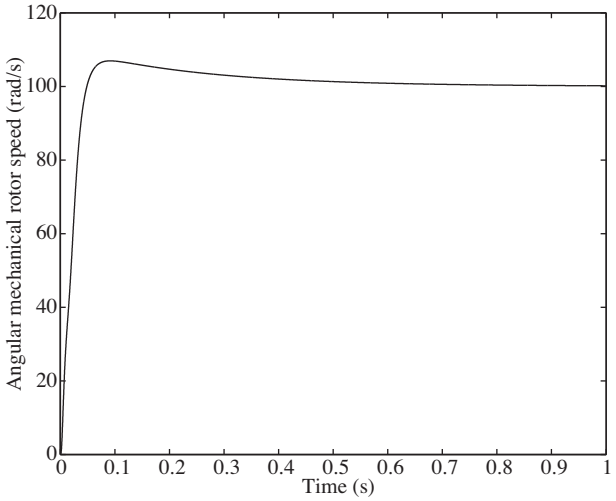

Figure 11. Speed of the rotor in assumed induction motor under robust control.

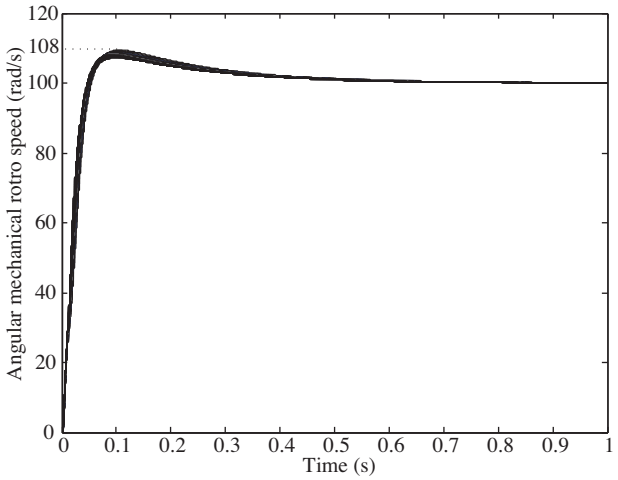

Figure 12. Speed of the rotor for the rotor and stator resistances variation up to 100% and 50%, respectively.

8. Conclusions

In this paper, we have introduced a robust PI controller design procedure for induction motors that guarantees robust stability and performance of the nonlinear induction motor. First we derived useful equations in order to demonstrate the stability and performance conditions of the system including the PI controller, by assuming that the whole derived models of the induction motor are minimum-phase. We then obtained specific regions of the $k_p - k_i$ plane to achieve the aforementioned goals. Using all these conditions, the relations between frequency-domain characteristics and the performance of the designed controllers were validated by simulations using MATLAB software. Other than ensuring the robust stability and performance of the closed-loop system, the proposed method provides a systematic approach to design PI controllers for an induction motor and could be used to easily compute the stability region. The design procedure method can also specify regions as search spaces for intelligent optimization methods to optimize the coefficients of the PI controllers. It is recommended that further research be undertaken to implement this control methodology and analyze its performance.

References

[1] Krause PC, Wasynczuk O, Sudhoff SD. Analysis of Electric Machinery and Drive Systems. 2nd ed. New York, NY, USA: Wiley-IEEE Press, 2002.

[2] Marino R, Tomei P, Verrelli C. A global tracking control for speed-sensorless induction motors. Automatica 2004; 40: 1071–1077.

[3] Lipo TA. Vector Control and Dynamics of AC Drives. New York, NY, USA: Oxford University Press, 1996.

[4] Leonhard W. Control of Electrical Drives. New York, NY, USA: Springer-Verlag, 1996.

[5] Ho EY, Sen PC. Decoupling control of induction motor drives. IEEE Ind Electron M 1988; 35: 253–262.

[6] Jansen PL, Lorenz RD, Novotny DW. Observer-based direct field orientation: analysis and comparison of alternative methods. IEEE Ind Appl Mag 1994; 30: 945–953.

[7] Benchaib A, Rachid A, Audrezet E. Sliding mode input-output linearization and field orientation for real-time control of induction motors. IEEE T Power Electr 1999; 14: 3–13.

[8] Wai RJ, Lin KM. Robust decoupled control of direct field-oriented induction motor drive. IEEE Ind Electron M 2005; 52: 837–854.

[9] Ma Z, Zheng T, You X. A new sliding-mode current controller for field oriented controlled induction motor drives. In: 31st Annual Conference of IEEE Industrial Electronics Society (IECON 2005); November 2005; Raleigh, North Carolina, USA. New York, NY, USA: IEEE. pp. 1341–1346.

[10] Meroufel A, Massoum A, Wira P. A fuzzy sliding mode controller for a vector controlled induction motor. In: IEEE International Symposium on Industrial Electronics (ISIE 2008); June 2008; Cambridge, UK. New York, NY, USA: IEEE. pp. 1873–1878.

[11] Yang SM, Lee CH. A deadbeat current controller for field oriented induction motor drives. IEEE T Power Electr 2002; 17: 772–778.

[12] Bousserhane I, Hazzab A, Sicard P, Rahli M, Mazari B, Kamli M. Fuzzy sliding mode based on indirect field orientation for induction motor drive. In: 32nd Annual Conference on IEEE Industrial Electronics (IECON 2006); November 2006; Paris, France. New York, NY, USA: IEEE. pp. 537–542.

[13] Moallem M, Mirzaeian B, Mohammed O, Lucas C. Multi-objective genetic-fuzzy optimal design of PI controller in the indirect field oriented control of an induction motor. IEEE T Magn 2001; 37: 3608–3612.

[14] Montanari M, Peresada S, Tilli A. A speed-sensorless indirect field-oriented control for induction motors based on high gain speed estimation. Automatica 2006; 42: 1637–1650.

[15] Ba-Razzouk A, Cheriti A, Olivier G. A neural networks based field oriented control scheme for induction motors. In: Industry Applications Conference 1997. Thirty-Second IAS Annual Meeting (IAS'97); October 1997; New Orleans, LA, USA. New York, NY, USA: IEEE. pp. 804–811.

[16] Tan N, Atherton DP. Design of stabilizing PI and PID controllers. Int J Syst Sci 2006; 37: 543–554.

[17] Tan N, Kaya I, Yeroglu C, Atherton DP. Computation of stabilizing PI and PID controllers using the stability boundary locus. Energ Convers Manage 2006; 47: 3045–3058.

[18] Ravi TA, Chakraborty C, Maiti S, Hori Y. A new model reference adaptive controller for four quadrant vector controlled induction motor drives. IEEE Ind Electron M 2012; 59: 3757–3767.

[19] Wu B. High-Power Converters and AC Drives. New York, NY, USA: Wiley-IEEE Press, 2006.

[20] Doyle JC, Francis BA, Tannenbaum A. Feedback Control Theory. New York, NY, USA: Dover Publications, 2009.

[21] Bhattacharyya SP, Chapellat H, Keel LH. Robust Control: The Parametric Approach. Upper Saddle River, NJ, USA: Prentice Hall, 1995.

[22] Ghosh BK. Some new results on the simultaneous stabilizability of a family of single input, single output systems. Syst Control Lett 1985; 6: 39–45.

[23] Ho MT, Datta A, Bhattackaryya S. Design of P, PI and PID controllers for interval plants. In: Proceedings of the 1998 American Control Conference; June 1998; Philadelphia, PA, USA. New York, NY, USA: IEEE. pp. 2496-2501.

[24] Barmish BR, Hollot CV, Kraus FJ, Tempo R. Extreme point results for robust stabilization of interval plants with first-order compensators. IEEE T Automat Contr 1992; 37: 707–714.

[25] Huang YJ, Wang YJ. Robust PID tuning strategy for uncertain plants based on the Kharitonov theorem. ISA T 2000; 39: 419–431.

[26] Mitronikas ED, Safacas AN. An improved sensorless vector-control method for an induction motor drive. IEEE Ind Electron M 2005; 52: 1660–1668.

[27] Cho J. Multiple modeling and control of nonlinear systems with self-organizing maps. PhD, University of Florida, Gainesville, FL, USA, 2004.